Check for updates

Received: 22 June 2021 | Accepted: 23 September 2021

DOI: 10.1002/pamm.202100139

Efficient simulation of heterogeneous materials with the finite cell method

Mahan Gorji[1,*] and **Alexander Düster**[1]

[1] Hamburg University of Technology, Numerical Structural Analysis with Application in Ship Technology (M-10), Am Schwarzenberg-Campus 4 (C), 21073 Hamburg

The finite cell method (FCM) represents a combination of high-order finite elements with the fictitious domain approach. Due to it's simple mesh generation the FCM reduces the pre-processing effort. For heterogeneous problems of solid mechanics however, discontinuities occur at the material interfaces, which cannot be captured by the smooth shape functions of the FCM anymore, whereby the convergence deteriorates. Thus, to recover the optimal convergence rate, we extend the FCM ansatz by specially designed shape functions, which are able to capture discontinuities at the material interfaces. To get more insight into the problem, we study the performance of the proposed method by means of a two-dimensional example.

© 2021 The Authors. *Proceedings in Applied Mathematics & Mechanics* published by Wiley-VCH GmbH.

1 Local enrichment for problems with heterogeneous materials

The finite cell method (FCM) is a numerical method for solving problems in solid mechanics. Unlike the finite element method (FEM), it uses a Cartesian mesh for the discretization of the problem and introduces the geometry of the problem by means of an indicator function during the integration of the weak form. The FCM exhibits high convergence rates for problems with smooth solutions, e.g. for a plate with a circular hole [1].
If the problem is heterogeneous, i.e. it consists of multiple domains with different materials, discontinuities will occur at the material interfaces. For problems in solid mechanics these discontinuities correspond to kinks in the displacement field and jumps in the strain field. For such problems the standard FCM is not sufficient anymore, because it approximates the discontinuity by high-order smooth shape functions, which leads to oscillations [2]. Therefore, the ansatz is extended by discontinuous shape functions, which capture the non-smooth part of the solution and are only applied in locally defined regions. This extension of the FCM - called local enrichment - exhibits high convergence rates, while the additional number of degrees of freedom is kept low [2]. In this paper, we perform further simulations with the aim of getting a deeper understanding of the problem and it's solution method. In this context, we also investigate the influence of the numerical integration. For our simulations, we utilize the high-order partition of unity (PUM) approach combined with the hp-d concept, which results in the hp-d/PUM-FCM [2]. The main idea is to extend the ansatz as follows

$$\mathbf{u}_{hp\text{-}d/\mathrm{PUM}} = \underbrace{\sum_{i=1}^{n} N_i \, \mathbf{U}_i}_{\text{base}} + \underbrace{\sum_{i=1}^{n^*} N_i^* F \, \mathbf{a}_i}_{\text{enrichment}} , \tag{1}$$

where the first term (denoted as *base*) captures the smooth part of the solution using n high-order shape functions N_i of order p and is applied in the whole domain. In contrast, the second term (denoted as *enrichment*) is only applied in local regions, where the solution is discontinuous. Here, n^* high-order smooth shape functions N_i^* of order p_e are used, which build a partition of unity. Their corresponding additional degrees of freedom are denoted as $\mathbf{a}_i$. The non-smooth part of the solution is captured by the enrichment function $F(\mathbf{x})$, which is constructed through the modified abs-enrichment [3]

$$F(\mathbf{x}) = \left| \sum_{i=1}^{n_F} M_i \, \phi_i \right| - \sum_{i=1}^{n_F} M_i \, |\phi_i| \, . \tag{2}$$

Here, M_i are partition of unity functions of order p_F and $\phi(\mathbf{x})$ is the level-set function describing the material interface. This enrichment function has the advantage that it captures the material interface as well as vanishes at the boundary of the local regions. Finally, we only enrich cells which are cut by the material interface, mentioned as the *cell-wise* approach.

2 Numerical example

A plate with a circular inclusion, as depicted in Fig. 1 (a), is subjected to prescribed displacements. The structure is in plain strain condition and has a radius of $a = 3$ and a side length of $2c = 16$. A linear elastic material model is used, where the plate has a Young's modulus of $E_{\mathrm{plate}} = 10^4$ and a Poisson's ratio of $\nu_{\mathrm{plate}} = 0.3$, while the inclusion has a Young's modulus of

* Corresponding author: e-mail mahan.gorji@tuhh.de, phone +49 40 42878 6099

This is an open access article under the terms of the Creative Commons Attribution License, which permits use, distribution and reproduction in any medium, provided the original work is properly cited.

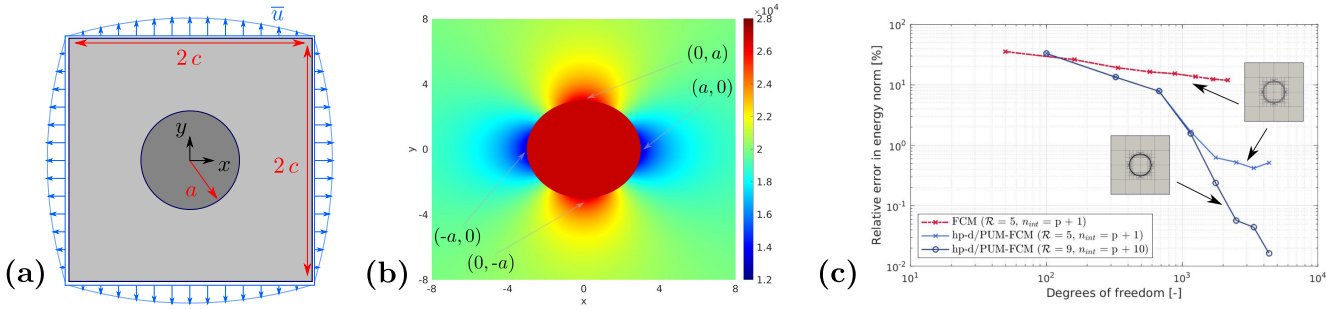

Fig. 1: Plate with a circular inclusion. (a) Setup. (b) Analytical solution σ_{yy}. (c) Convergence study with $p = p_e = 1, \ldots, 8$.

$E_{\text{inc}} = 10\, E_{\text{plate}}$ and a Poisson's ratio of $\nu_{\text{inc}} = \nu_{\text{plate}}$. This benchmark, which was motivated by [4], provides an analytical solution of the displacement field, from which the stresses are derived. The σ_{yy}-component of the stress results in

$$\sigma_{yy}(x,y) = \begin{cases} C & \sqrt{x^2+y^2} \leq a \\ A - B\frac{x^2-y^2}{(x^2+y^2)^2} & \text{otherwise}\,, \end{cases} \tag{3}$$

where $A = 1.992031872509961 \cdot 10^4$, $B = 6.205945448973371 \cdot 10^4$ and $C = A + \frac{B}{a^2} = 2.681581366840209 \cdot 10^4$. As it can be seen in Fig. 1 (b), σ_{yy} is continuous at the points $(0, \pm a)$, while it exhibits a jump at the points $(\pm a, 0)$. The reason is that for the stress field, continuity must be maintained only in normal direction, not necessarily in tangential direction. Note that the inclusion is ten times stiffer than the plate, therefore the stress inside the inclusion is higher. The structure is discretized using 4×4 finite cells, on which the numerical integration is performed using a quadtree with tree-depth $\mathcal{R}$ and n_{int} integration points in every unit direction. Since the circular inclusion can be described by a quadratic level-set function, $p_F = 2$ is sufficient for the enrichment function. Boundary conditions are applied using the weak penalty method with a penalty factor of $\beta = 10^{20}$ [5]. The results are shown in Fig. 1 (c), where in a p-refinement the error in energy norm is plotted over the number of degrees of freedom. The reference strain energy is given as

$$\mathcal{U}_{\text{ref}} = 4.959409735463204 \cdot 10^6\,. \tag{4}$$

While the standard FCM exhibits a very poor convergence (red curve), the *hp-d*/PUM-FCM - first with a low integration accuracy ($\mathcal{R} = 5$, $n_{\text{int}} = p + 1$) - significantly improves the convergence behavior (light blue curve). Since the relative error stagnates for $n_{\text{DOF}} > 1000$, the integration needs to be further improved. By doing so, the *hp-d*/PUM-FCM with a high integration accuracy ($\mathcal{R} = 9$, $n_{\text{int}} = p + 10$) converges very fast (dark blue curve). The corresponding stress component σ_{yy} is presented in Fig. 2 (a) - (c). The FCM alone is not able to capture the jump in the stress and thus, oscillations occur. In comparison, the *hp-d*/PUM-FCM captures the jump very precisely, but with the low integration accuracy, there are still some fluctuations. Further rising the accuracy of the integration, the fluctuations vanish and the solution quality is improved.

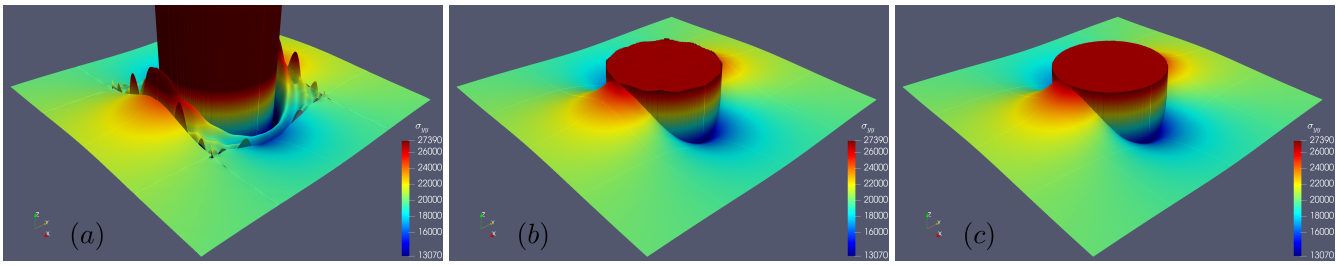

Fig. 2: Stress σ_{yy} for $p = p_e = 8$. (a) FCM. (b) *hp-d*/PUM-FCM ($\mathcal{R} = 5$, $n_{\text{int}} = p + 1$). (c) *hp-d*/PUM-FCM ($\mathcal{R} = 9$, $n_{\text{int}} = p + 10$).

Acknowledgements The authors gratefully acknowledge the support provided by the DFG (Deutsche Forschungsgemeinschaft) under the grant number DU 405/17-1. Open access funding enabled and organized by Projekt DEAL.

References

[1] M. Dauge, A. Düster and E. Rank, J. Sci. Comput. **65**, 1039–1064 (2015).
[2] M. Joulaian and A. Düster, Comput. Mech. **52**, 741–762 (2013).
[3] N. Moës, M. Cloirec, P. Cartrauda and J.-F. Remacle, Comput. Methods Appl. Mech. Engrg. **192**, 3163-3177 (2003).
[4] J. Schröder, T. Wick, S. Reese et al., Arch. Computat. Methods. Eng. **28**, 713-751 (2021).
[5] T.-P. Fries and T. Belytschko, Int. J. Numer. Meth. Engng. **84**, 253-304 (2010).

© 2021 The Authors. *Proceedings in Applied Mathematics & Mechanics* published by Wiley-VCH GmbH.